# Energy-Efficient RF-Optics Multi-Beam Systems Using Correlation Technologies: Toward Hybrid GaN-FDSOI Front-End-Modules

S. Wane[$], F. Ferrero[^], J. Sombrin[$], L. Tombakdjian[$], D. Bajon[$], P. Ratajczak[#], F. Molina[⊥], M. Rack[†], L. Nyssens[†], J.-P. Raskin[†], D. Lederer[†], C. Craeye[†], G. Albertini[Σ], V. Huard[*], P. Poilvert[§], C.-A. Tavernier[§], D. Floriot[§]

[$]eV-Technologies, [^]LEAT-CNRS, [#]ORANGE-Labs, [⊥]Rohde & Schwarz,
[†] ICTEAM-UCL, [Σ]MathWorks-France, [*]Dolphin-Design, [§]UMS-RF

2022 IEEE Texas Symposium on Wireless and Microwave Circuits and Systems (WMCS) | 978-1-6654-8609-5/22/$31.00 ©2022 IEEE | DOI: 10.1109/WMCS55582.2022.9866246

***Abstract*— In this paper, we propose hybrid GaN-FDSOI Front-End-Modules (FEMs) combined with lens-based mmWave antenna modules for energy-efficient multi-beamforming systems. X-topology Lattice-based balanced (LB) and unbalanced (LU) differential switches are designed and fabricated using FDSOI platforms for building scalable multi-beamforming FEMs. Unified mmWave and Baseband correlation technologies based on energy density and EVM (*Error Vector Magnitude*) metrics are introduced for low complexity (*leveraging sparsity of MIMO channels*) cost-effective multi-beamforming systems. Combination of convolutional accelerators with analog signal processing for linking beam-selection algorithms to *stochastic-wave-shaping (SWS)* will create new paradigms for eliminating the concept of "*elements*" in arrays and replacing it by the vision of "*radiating current flows*" over a textured surface (*metasurface* or *metavolume*). The radiating metasurfaces or metavolumes which can be conformal to the patterned optical lenses are fed by a limited number of emitting/receiving points. The use of time-modulated correlation functions will foster new system architectures with critical functionalities including direction of arrival (DOA) estimation and secure communications.**

**Keywords— Hybrid GaN-FDSOI, Correlation Functions, Multi-Beamforming, EVM, X-Topology switches, Patterned Lenses, ASIC, FPGA, Power-Density (PD), Direction of Arrival.**

## I. INTRODUCTION

We introduce energy-efficient cost-effective and low complexity solutions for mmWave beamforming systems taking advantage of hybrid GaN-FDSOI technologies (Fig.1) backed-up by the following enablers:

- *mmWave-Optical multi-beam* [1-2] using Correlation technologies [3] for the characterization of stochastic fields: by using angle-dependent energy-density focusing capability of optical lenses, low-consumption and low complexity beamformer front-end-module.
- *Lattice-based balanced and unbalanced switching architectures* for multi-beamforming front-end-modules Fig.1(a-b) [4]: fully-differential multi-port scalable SPST and SP4T switches are designed with wideband [4-5] operation (DC up to 50 GHz) using FDSOI platforms.
- *Correlation-based EVM* [6-9] *metrics*, for single-beam and multi-beam systems, compliant with ASIC and FPGA implementation, using advanced convolutional accelerators [3]. Combination of convolutional accelerators with analog signal processing for linking beam-selection algorithms to SWS is proposed.

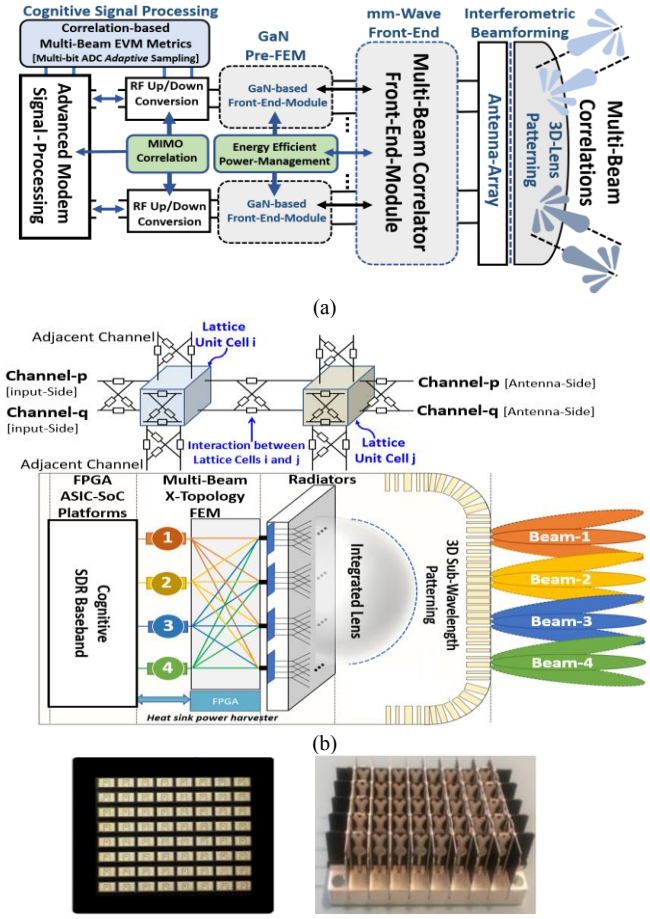


Fig.1. Hybrid GaN-FDSOI Front-End-Modules (a) including correlation-based EVM signal processing for multi-beamforming systems (b) including Antenna-array module in single (c) and dual (d) polarizations, co-integrated with patterned 3D-Lens.

This contribution presents practical realization of hybrid GaN-FDSOI based beamformers combining switched correlator FEMs with patterned 3D lenses for low-complexity energy-efficient solutions. Correlation technologies are introduced both at RF/mmWave and baseband frequencies for OTA testing of mobile devices and systems. Perspectives for correlation-based EVM measurement of multi-beam systems are drawn for deployment in FPGA and ASIC platforms, beyond the scope of the new IEEE P1765 standard [9]. The proposed lens-based mmWave multi-beam beamformers, in offering sparse properties in both time and angular dimensions, provide significantly reduced signal

978-1-6654-8609-5/22/$31.00 ©2022 IEEE

processing which result in a small set of correlation-based RF measurements for channel estimation of MIMO systems. Mosaic partitioning strategies, *exploiting the sparsity of MIMO correlation matrix*, open new possibilities for combining multiple arrays into a full array state (FAS) to form one single beam, or for using them to form separate beams in the sub-array state (SAS). Space-time pulse shaping strategies will foster new energy-efficient modulated amplitude (AM) and phase (PM) waveforms that can be accurately and separately engineered to meet critical OTA performances. The AM and PM waveforms may be dynamically modulated in a predefined manner by properly mapping pulse train sequences to desired beamforming characteristics. The optimization of desired beamforming characteristics covering the carrier signal and its harmonic components can benefit from built-in convolutional accelerators for *RF embodied cognitive signal processing*.

## II. Analysis and Discussion

### *A. Correlation Technologies Using Power-Density and Energy-Density Metrics for Stochastic Gaussian Beams*

The combination of switched correlator front-end-module with 3D patterned lens, in addition to providing multibeam functionality, enables architecture solutions where time-modulated radiators (*conventional antenna arrays or metasurfaces*) can transmit or receive signals modulated by wave-shaped time pulses. The wave-shaped time pulses are specified using configurable sequences to control the antenna radiation pattern accounting for the rise and fall time of the switching devices. Broadband power-level dependent physics-based RLC [4] circuit synthesis compliant with Four-Terminal devices, are combined with antenna tuning control and regulation available in FD-SOI technologies. Beyond standard figures of merits used for qualifying classical SPDT switches [10], new requirements in relation with time and frequency domains correlation based on new metrics accounting for radiation effects (*e.g., non-reflective smart-loading*) and power-dependent harmonic signatures (*e.g., TDD operation*) are used. The resulting flexibility offers a broad range of applications including radar sensing and the control of stochastic signals. This flexibility (*adaptive transceiver*) can be operational for optimizing multi-user interferences and for blind denoising or decorrelating [5] received signals from each other in jammer configurations by exploiting correlation technologies. Using Luneburg's vector diffraction theory and Fresnel approximations, an analytical model for the on-axis transverse and longitudinal electric fields and associated intensity distributions is derived. Let's assume the following signals from a point source residing at angle θ and received on two antennas separated by a baseline D:

$$\begin{aligned} S_1(t) &= cos\left[2\pi\left(F_0 t + \tfrac{K}{2}t^2\right)\right] + n_1(t) \\ S_2(t) &= cos\left[2\pi\left(F_0(t-\tau_g) + \tfrac{K}{2}(t-\tau_g)^2\right)\right] + n_2(t) \end{aligned} \quad (1)$$

where $F_0$ is the carrier frequency, K (Hz/s) is the chirp rate, and $\tau_g = (D/c)\sin(\theta)$ designates the geometrical time delay of the wavefront between the two antenna elements. The in-phase component of the cross-correlation of the two received signals can be expressed as:

$$\begin{aligned} &C_{S_1S_2}(\tau_g) = \\ &\left\langle cos\left[2\pi\left(F_0 t + \tfrac{K}{2}t^2\right)\right] \left| cos\left[2\pi\left(F_0(t-\tau_g) + \tfrac{K}{2}(t-\tau_g)^2\right)\right]\right\rangle \\ &\quad = cos\left[2\pi\left(F_0 + Kt - \tfrac{K}{2}\tau_g\right)\tau_g\right] \end{aligned} \quad (2)$$

The noise terms are suppressed as they are assumed uncorrelated with each other and with the received signals.

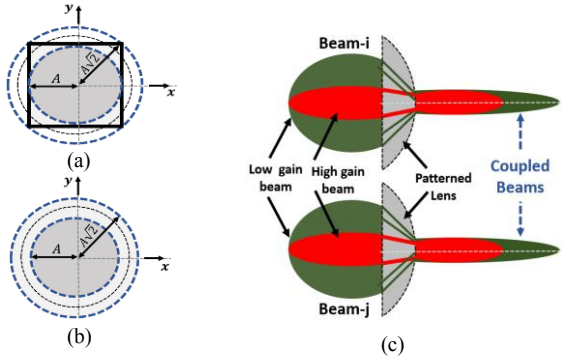


Fig. 2. Square (a) and circle-shaped (b) averaging surfaces for PD extractions of Gaussian beams. Patterned lens with distributed gain beams (c).

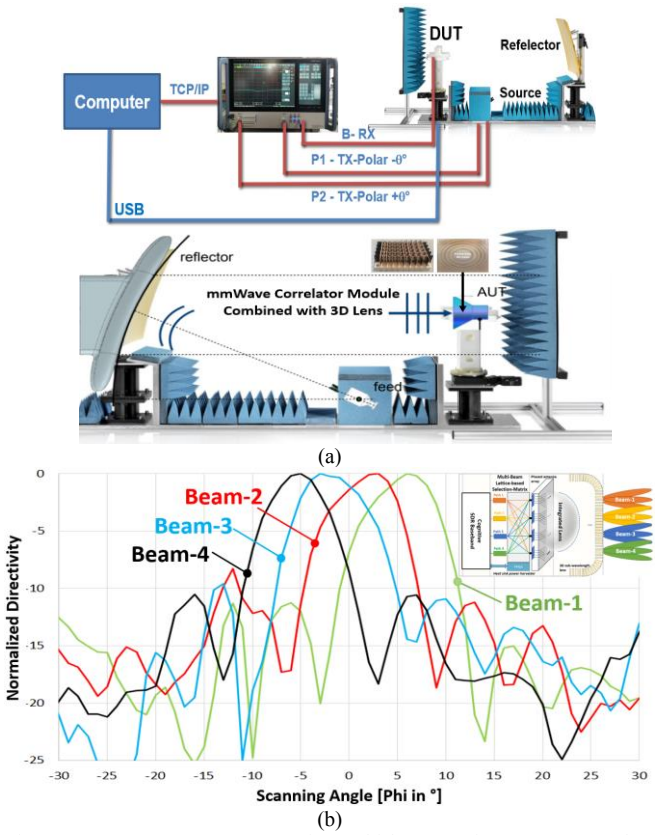


Fig.3. CATR measurement setup for multi-beam testing (a), measured 4-beam system at 26 GHz (b).

TABLE I: STATE-OF-THE-ART MM-WAVE SWITCH MODULES IN SOI TECHNOLOGY

| *Simulated data | [15] 2017 | [16] 2017 | [17] 2018 | [13] 2020 | [14] 2020 | This Work 2021 | | |
|---|---|---|---|---|---|---|---|---|
| Technology | 130nm SOI | 45-RFSOI | 22FDX® | 22FDX® | 45-RFSOI | 22FDX® | | |
| Type | SPDT Single-Ended | SPDT Single-Ended | SPST Single-Ended | SPDT Single-Ended | SPST Differential | SPST Differential | SP4T Differential | |
| Topology | Series-Shunt with matching | Series-Shunt | Series-Shunt | Series-Shunt with matching | Lattice Balanced [LB] | Lattice Un-balanced [LU] | Lattice Balanced [LB] | |
| Band | DC-50 | DC-50 | DC-40 | DC-40 | DC-43 | DC-35 | DC-50 | DC-40 |
| IL (28 GHz) [dB] | 1.0 | 0.7 | 1.1 | 1.66 | 2.5 | 1.55 | 1.92 | 2.65 |
| ISO (28GHz) [dB] | 32 | 24 | 24 | 33.4 | 57 | 21 | 53 | 48.5 |
| P1dB [dBm] | 14 | 29.5 | 23 | 20.5 | 19.6 | 24.9* | 23.5* | 23.2* |
| IIP3 [dBm] | 27 | 46 | 43 | 38.5 | 25.5 | 52.2* | 47.6* | 42.2* |
| Device Size [$10^{-3}$ mm$^2$] | 40 | 4 | / | 34 | 5.8 | 7.1 | 7.1 | 35 |

After low pass filtering, the higher frequency carrier components are rejected. By combining the in-phase and quadrature outputs of the cross-correlation function leads to the following complex signal response:

$$r(\tau_g) = Exp\left[j2\pi\left(F_0 + Kt - \frac{K}{2}\tau_g\right)\tau_g\right] \quad (3)$$

This complex signal can be used, based on linear frequency modulated transmitters combined with receivers composed of interferometric array with n elements, to extract the angle of up to O(N$^2$) targets. For the n elements, the correlation matrix in the frequency domain can be expressed as a function of the time-windowed signal $S_T(t)$ using Fourier transform ($\mathcal{F}$):

$$C(\omega) = \mathcal{F}\{\langle S_T(t)|S_T^{\dagger}(t+\tau)\rangle\} \quad (4)$$

The complex power-density is extracted from the Gaussian beam using the following equations where $\rho$ and $z$ respectively represent the radius and the distance from the DUT:

$$P_{Density}(\rho, z) = P_0 \frac{W_0}{W(z)} exp\left(-\frac{\rho^2}{W^2(z)}\right)\kappa(z) \quad (5)$$

$$\kappa(z) = exp\left(-ik\frac{\rho^2}{2R(z)} + i\zeta(z)\right) \text{ representing the phase.}$$

Semi-analytical expressions can be obtained from equation (5) for extracting averaged power-density over regular surfaces in Fig. 3 (a-b) using the following integrals (Fig.2):

$$\iint_{R_A} exp(-\rho^2)\rho d\rho d\theta = \int_0^A \int_0^{2\pi} \rho exp(-\rho^2) d\rho d\theta \quad (6)$$

$$= \int_0^A \rho exp(-\rho^2) d\rho \times \int_0^{2\pi} d\theta = 2\pi\left[-\frac{1}{2}exp(-\rho^2)\right]_0^A$$

$$= \pi\left(1 - exp(-2A^2)\right)$$

Fig. 3(a) shows a CATR [11] setup used for testing the proposed multi-beamforming system. The CATR features a reflector to minimize the space requirements for OTA tests. In Fig.3 (b), measured 4-beam configuration operating at 26 GHz is presented. The beam switching front-end-module uses *eVT-3016* mmWave correlator module. The *eVT-3016,* with USB controlled crossover switch-matrix, can switch any of two or four common ports to any of 16 input/output channels. It features a full crossover capability allowing any switching combination to be selected while supporting bi-directional RF paths from 16 kHz to 30 GHz. *UMS*-based GaN [12] front-end-module is used to drive the *eVT-3016* correlator in TX and RX modes. Antenna-in-Package (AiP) co-assembled with 3D Patterned Lenses benefits from fully-differential multi-port scalable SPST and SP4T switches in Fig.4 and Fig.5 for MCM integration solution. Fig.4 illustrates a two-port dual-beam (*beams i and j among 64 channels*) using unitary antenna elements separated by a variable distance d.

The fully differential switches in Fig.5 use lattice-based balanced and unbalanced architectures with performances summarized in Table I in comparison with state-of-the-art switch [10] modules in SOI technology [13-17]. The differential mode blocking topology is presented in Figure 5.

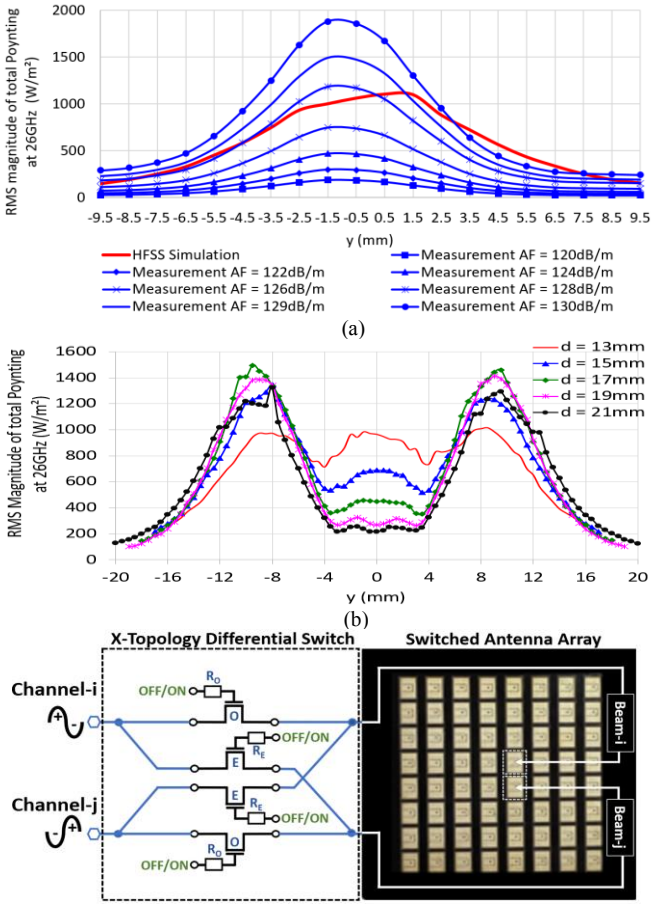


Fig.4: Power-Density Single (a) and Dual-Beam (b) Couplings as function of separation distance d. X-topology architecture for switched dual-beam synthesis (c) in O and E states excitation/sensing.

When a differential input signal is applied between nodes $a_1$ and $a_2$, in Fig. 5(g), the differential output signal (between nodes $b_1$ and $b_2$) is perfectly equal to zero if the four branch impedances are equal. Let branches 1 and 2 be the *direct branches* (D) of admittance $Y_D$, and branches 3 and 4 be the *crossed branches* (X) of admittance $Y_X$. Each branch impedance is implemented using a series stack of three 22FDX® SLVT NFETs (with 20 nm gate length, targeting

above 20 dBm of power handling. In the ON state, branches 1 and 2 are turned on by applying a front gate bias of $V_g = 0.9$ V and a back-gate bias of $V_{bg} = 3$ V while branches 3 and 4 are turned off with $V_g = -0.9$ V and $V_{bg} = 0$ V. In that case $Y_{D\text{-}ON}$ is high and $Y_{X\text{-}OFF}$ is low and $Y_{21\text{-}ON}$ reduces to $-Y_{D\text{-}ON}/2$. In the OFF state, all branches are turned off. Then, $Y_{21\text{-}OFF}$ becomes $(Y_{X\text{-}OFF} - Y_{D\text{-}OFF})/2$. If the branch impedances are equal, destructive interference occurs between the signal passed through the D branches and the anti-phase signal passed through the X branches, and $Y_{21} = 0$.

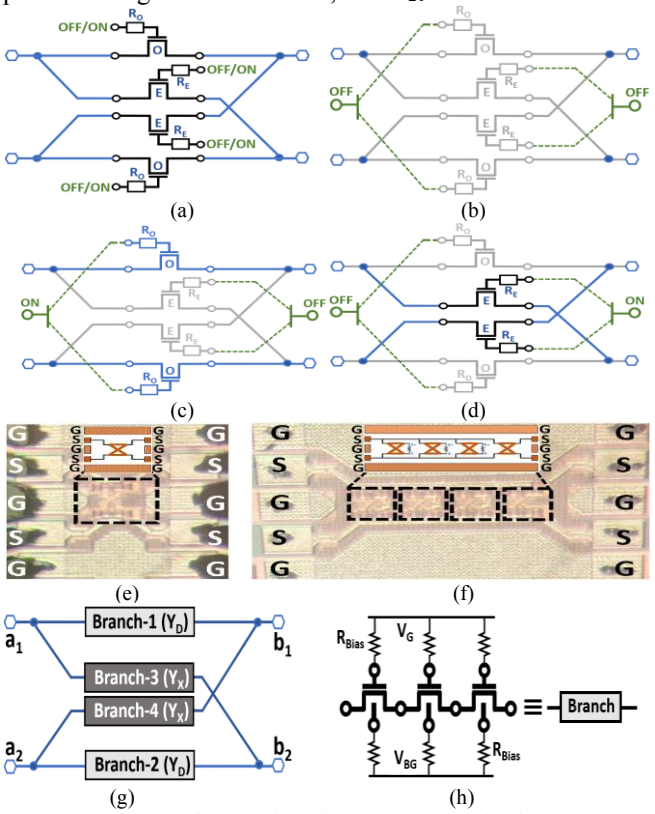


Fig. 5. Diagrams (a), (b), (c), (d), and microscope (e), (f) photos of unitary Lattice- Cell switches. X-Topology architecture (g) with stacked FETs (h).

The canonical O and E states of the X-Topology unitary switching cell are characterized by their two-port S-parameter matrix $[S_{Two-Port}]$:

$$[S_{Two-Port}] = \frac{\Gamma_{Even}}{2}\begin{bmatrix}1 & 1\\ 1 & 1\end{bmatrix} + \frac{\Gamma_{Odd}}{2}\begin{bmatrix}1 & -1\\ -1 & 1\end{bmatrix} \quad (7)$$

$S_{Two-Port} = S_{ON}^{O-E}$ and $S_{Two-Port} = S_{OFF}^{O-E}$ when O and E states are respectively both activated or both disactivated. The individual states $S_{ON}^{O}$ and $S_{ON}^{E}$ respectively correspond to the O and E states in activation mode and the other one disactivated. By construction, the X-topology switching unit cell provides *broadband 180° phase-shifting* which is beneficial for correlator circuits and phased-array applications. Furthermore, the handled signals are differential for robustness to EMC/EMI interferences. A SPICE-based nodal representation can be derived based on the following admittance relation linking the currents $I_A$ and $I_C$ to the differential voltages $V_A - V_B$ and $V_C - V_D$:

$$\begin{bmatrix}I_A\\ I_C\end{bmatrix} = \frac{1}{2}\begin{bmatrix}{Z_{Trans}}^{-1} + {Z_{Long}}^{-1} & {Z_{Trans}}^{-1} - {Z_{Long}}^{-1}\\ {Z_{Trans}}^{-1} - {Z_{Long}}^{-1} & {Z_{Trans}}^{-1} + {Z_{Long}}^{-1}\end{bmatrix}\begin{bmatrix}V_A - V_B\\ V_C - V_D\end{bmatrix} \quad (8)$$

$Z_{Trans} = z_{ref}\frac{1+\Gamma_{Even}}{1-\Gamma_{Even}}$ and $Z_{Long} = z_{ref}\frac{1+\Gamma_{Odd}}{1-\Gamma_{Odd}}$ respectively refer E (*even*) and O (*odd*) states ($z_{ref}$ *being a reference impedance*). Extension of the SPICE representations to include multi-harmonic components and radiation effects is proposed. Several X-topology delay-line [5] design solutions with distributed ground references in Fig.5 are fabricated and experimentally evaluated in terms of their broadband RF performances.

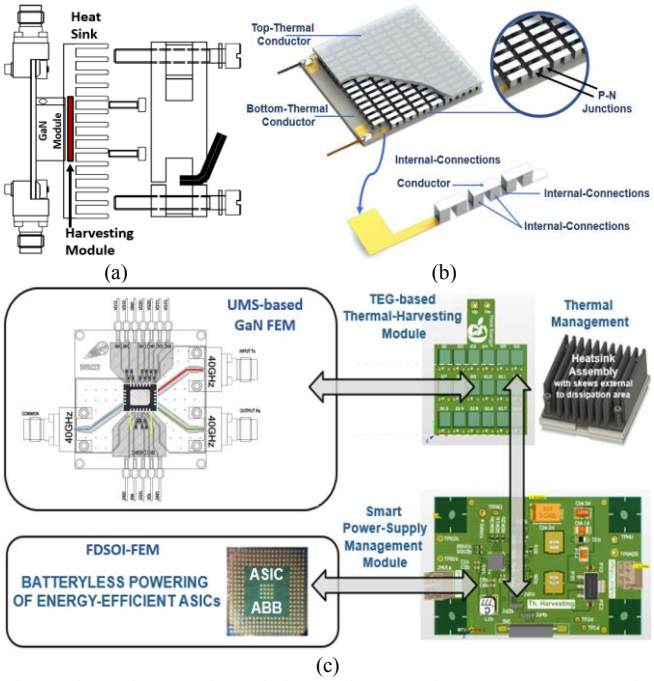


Fig. 6. Thermal-Harvesting solution (a) for RF and mmWave GaN-FEM for batteryless powering of energy-efficient ASICs. Seebeck-Module (b) integrating P-N junctions. Use-case based on UMS-based GaN FEM (c).

The extraction of the energy-density using correlation function is reported at 26 GHz. Adaptive-Body-Biasing (ABB) available in FDSOI technologies helps containing PVT (*Process-Voltage-Temperature*) related variations. The ABB functionality at switch device level uses stacked transistors represented by four effective terminals: source, drain, gate, and body – the volume underneath the conduction channel. By regulating a voltage bias on this fourth terminal, the transistor's threshold voltage can be accurately controlled for improved RF performance, reduced energy consumption and process spread. Consequently, nonlinear optimizations can be conducted for the shape of switching waveforms to be synthesized accounting for the impact of harmonic generations on radiation patterns. Such nonlinear optimizations strongly benefit from the energy-efficiency

resulting from the low-complexity sparse [18] architecture solutions. The lower gain obtained by fewer radiating elements linked to the sparse architecture is compensated by a 3D-patterned lens directly integrated with the radiators (antenna array or metasurface/metavolume). Compared to classical phased array systems, the power consumption of the digital and RF part will be divided by *a reduction factor higher than 10*. A detailed calculation of budget link and power consumption for different scenarios is provided in Table II showing the advantages of the proposed architecture solutions compared to classical phased-array [20-21] systems. In the present version of the proposed lenses, in Tab.II, the parameter $\kappa$=1 for the scanning angle. Ongoing developments are expected to significantly increase this value. Furthermore, the unique capability to generate independent beams enables higher throughput or multi-user application with real-time pattern optimization as a function of time [20], including harmonic generation, for transmitting multiple channels simultaneously using single carrier frequency. Fig.6 shows a modular thermal-harvesting solution enabling batteryless powering of energy-efficient ASICs. Co-design of RF and optical Front-End-Modules with energy-harvesting [19] functionality is proposed in advanced FDSOI technologies.

TABLE II: ENERGY-EFFICIENCY ASSESSMENT OF CLASSICAL PHASED-ARRAY VERSUS PROPOSED ARCHITECTURE SOLUTION FOR 64 CHANNELS.

| Baseline Metrics | Classical mmW Phased-Array | Proposed Solution for 1 RF Path | Proposed Solution for 4 RF Path |
|---|---|---|---|
| Dimensions | *5*5*5 cm* | *10*10*~10cm* | *10*10*~10cm* |
| Antenna Elements | *64* | *64* | *64* |
| Tx EIRP Without GaN | *54 dBm* | *48 dBm* | *48 dBm per path* |
| **Tx EIRP with GaN** | ***59 dBm*** | ***53 dBm*** | ***53 dBm per path*** |
| Rx gain | *23dB* | *29dB* | *29dB* |
| **Total Tx+Rx without GaN** | ***78dB*** | ***77dB*** | ***77dB*** |
| Total Tx+Rx with GaN | *83dB* | *82dB* | *82dB per path* |
| Activated Elements | *64* | *4* | *16* |
| **RF Power Consumption** | **10W** | **0.6W** | **2.4W** |
| Scan-Angle | *+/- 60°* | *+/- κ×15°* | *+/- κ×15°* |
| Number of Beams | *1* | *1* | *4* |

### *B. Correlation-based EVM Metrics for Multi-Beam Systems*

Error Vector Magnitude (EVM) is used in modern communication standards to measure the overall degradation of the signal due to linear or nonlinear distortions, and to noise, interference and multipath impairments. The classical method for EVM (Error Vector Magnitude) computation is to compute vector errors between received ($y_n$) and ideal ($x_n$) symbols and then to compute a root-mean-square of the magnitude of these vectors for all symbols in a frame. For this, it is necessary to extract an optimum gain $\gamma$ (amplitude and phase) between received and ideal symbols that minimizes the EVM.

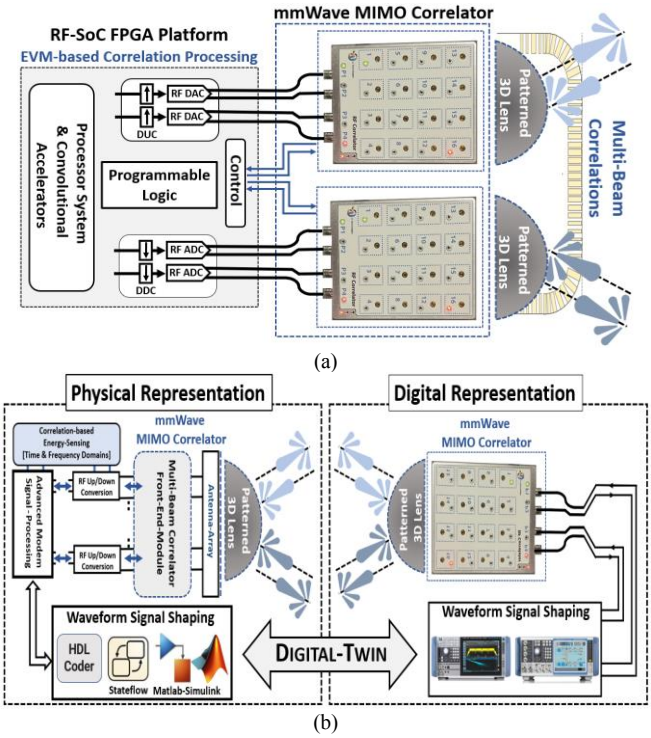


Fig.7. RF-SoC platform (a) compliant with MathWorks HDL-Coder for Correlation-based EVM real-time measurement. Digital-Twin (b) representation of mmWave MIMO system accounting for waveform signal shaping in time and frequency domains.

$$e_n = y_n - \gamma\, x_n \tag{9}$$

$$\sigma = \sqrt{\frac{1}{N}\sum_{n=1}^{N}|e_n|^2} = \sqrt{\frac{1}{N}\sum_{n=1}^{N}|y_n - \gamma x_n|^2} \tag{10}$$

$$\gamma = \frac{\sum_{n=1}^{N} y_n x_n^*}{\sum_{n=1}^{N} x_n x_n^*} \tag{11}$$

The optimum gain is computed by using autocorrelation and cross-correlation of ideal and received symbols. All these computations can be done in the following steps by replacing the optimum gain by its value and using the covariance between ideal $\boldsymbol{x}$ and received $\boldsymbol{y}$ symbols vectors.

$$cos\,\theta = \frac{\left|\sum_{n=1}^{N} y_n x_n^*\right|}{\sqrt{\sum_{n=1}^{N} y_n y_n^* \sum_{n=1}^{N} x_n x_n^*}} = \frac{|\langle y,x\rangle|}{\|y\|\|x\|} \tag{12}$$

$$EVM = \sqrt{\frac{1}{cos^2\,\theta} - 1} = tan\,(\theta) \tag{13}$$

EVM can be applied over the air (OTA) to each beam of a multibeam antenna and to each channel or the combination of channels of a MIMO transmission.

FPGA-based reconfigurable platform is proposed for OTA testing of multi-beamforming systems using *correlation-based EVM metrics*. The experimental setup uses automated MATLAB-based toolbox control modules combined with Rohde & Schwarz's mmWave signal generation and analysis for remote testing in time and frequency domains of stochastic signals. The flexibility offered by FPGA platforms enables versatile control and monitoring of the radiation properties, the radiation pattern, the polarizations, the

frequency band, the Direction of Arrival (DoA). The resulting platforms call for unification [23] of *modeling* and *measurement* into a coherent framework. The benefits of coherent measurement (instrumentation) and modeling (EDA tooling) solutions go beyond the simple need for productivity enhancement, and they open new possibilities for transforming apparent antagonisms between theory and experiment into necessary complementarities driving *Digital-Twin* in Fig.7(b) requirements (security, distributed information redundancy, Deep-Learning, AI inferences, etc.).

## III. Conclusion

In this paper, hybrid GaN-FDSOI front-end-module combined with a mmWave-Correlator module and RF-Optics [22] lens-based antenna-arrays have been proposed for building multi-beamforming systems. *Correlation technologies* are used for energy density based analysis of stochastic signals [3],[23]: this very specific way of transmitting/receiving EM waves will allow scanning directive multi-beam channels with *sparsely* distributed ports, i.e. with much fewer active electronic channels than in current state-of-the-art phased-array solutions. As a consequence, a much sparser sampling of the "*array*" and hence much lower consumption: *an improvement by a factor of 10 at least* is demonstrated. This low-complexity approach will drive next generation of communication and sensing systems eliminating the concept of "*elements*" in arrays and replacing it by the vision of "*radiating current flows*" over a textured surface (*metasurface* [24-25] or *metavolumes*) conformal to the patterned optical lenses that is fed by a limited number of emitting-receiving points. Lattice-based X-topology balanced (LB) and unbalanced (LU) differential switches are designed and fabricated using FDSOI [26] platform for building scalable multi-beamforming FEMs integrating *ABB* functionality for broadband waveform switching. Ongoing work is relative to the evaluation of beam squint effects which result from dispersive properties of lens dielectric materials both in transmit and reflect-arrays [27]. Perspectives for *Digital-Twin* platforms, with DSP-based convolutional-accelerators implemented at FPGA and ASIC levels (*preliminary implementations using HDL-Coder* [28]), are drawn for fast and accurate measurement of EVM for multi-beam steering systems. The overall arching Analog-Digital *SWS* leads to high security levels immune to blockage and jamming as the information is distributed through space-time and recovered using *several receivers* with embedded auto-correlation and cross-correlation processing.

## References


[1] R. Czarny, et al., "High permittivity, low loss, and printable thermoplastic composite material for RF and microwave applications", 2018 IEEE Conference on Antenna Measurements & Applications (CAMA), held in Västerås, Sweden, 3-6 Sep. 2018.

[2] X. Lleshi, R. Grelot, T. Q. Van Hoang, B. Loiseaux and D. Lippens, "Wideband Metal-Dielectric Multilayer Microwave Absorber based on a Single Step FDM Process," 2019 49th EuMC, pp. 678-681.

[3] Wane, et al., "Correlation Technologies for OTA Testing of mmWave Mobile Devices Using Energy Metrics", in Proc. of the 2022 IEEE Radio and Wireless Symposium (RWS), LA, USA 16-19 Jan. 2022.

[4] S. Wane et al., "Broadband Smart mmWave Front-End-Modules in Advanced FD-SOI with Adaptive-Biasing and Tuning of Distributed Antenna-Arrays," IEEE Texas Symposium on Wireless and Microwave Circuits and Systems, Waco, TX, USA, 2020, pp. 1-5.

[5] S. Wane et al., "Broadband Phase Control in Frequency and Time Domains: Design of True Delay-Lines for Noise-Decorrelation in Sensor-Arrays", ", IEEE-MTT-Texas symposium 2019.

[6] J. Sombrin, "Cross-correlation method measurement of error vector magnitude and application to power amplifier non-linearity performances", in Proceedings of ARFTG Austin, TX, USA 2016.

[7] J. Sombrin, "On the formal identity of EVM and NPR measurement methods: Conditions for identity of error vector magnitude and noise power ratio," in EuMC Proc. ,Manchester, UK, 2011, pp. 337-340.

[8] J. B. Sombrin, "Effective AM/AM and AM/PM curves derived from EVM measurements on constellations", to be published in Proceedings of ARFTG Denver, Colorado, USA 2022.

[9] https://standards.ieee.org/ieee/1765/10560/.

[10] M. Rack *et al*., *2020 IEEE Radio Frequency Integrated Circuits Symposium (RFIC)*, Los Angeles, CA, USA, 2020, pp. 67-70.

[11] https://www.rohde-schwarz.com/fr/produit/ats800b-page-de-demarrage-produits_63493-642314.html

[12] https://www.ums-rf.com

[13] H. Erkens and H. Heuermann, *IEEE Trans. on Microw. Theory and Techniques*, vol. 54, no. 6, pp. 2376-2382, June 2006.

[14] A. Eltaliawy, et al., *2020 IEEE Radio Frequency Integrated Circuits Symposium (RFIC)*, LA, CA, USA, 2020, pp. 63-66.

[15] B. Yu *et al*., *IEEE Transactions on Microwave Theory and Techniques*, vol. 65, no. 10, pp. 3937-3949, Oct. 2017.

[16] C. Li *et al*., *2018 IEEE 18th Top. Meet. on Silic. Monolith. Integrat. Circ. in RF Syst. (SiRF)*, Anaheim, CA, 2018, pp. 1-3.

[17] A. Balasubramaniyan et al., *2018 IEEE SOI-3D-Subthreshold Microelectronics Technology Unified Conference (S3S)*, Burlingame, CA, USA, 2018, pp. 1-2.

[18] ME. Lopes, "Unknown sparsity in compressed sensing: denoising and inference". IEEE Trans In Theory. (2016) 62:5145–66.

[19] S. Wane, "Thermo-electric harvesting and Co-Design strategies toward improved energy efficiency of emerging wireless technologies", Texas Symposium on Wireless and Microwave Circuits and Systems, 2018.

[20] R. W. Bickmore and R. Hansen, "Time versus space in antenna theory," Microwave scanning antennas, vol. 3, p. 15, 1966.

[21] P. Rocca, G. Oliveri, R. J. Mailloux, and A. Massa, ''Unconventional phased array architectures and design Methodologies—A review,'' Proc. IEEE, vol. 104, no. 3, pp. 544–560, Mar. 2016.

[22] S. Wane and N. Aflakian, "Photonics Chip-to-Chip Communication for Emerging Technologies: Requirements for Unified RF, mm-Waves and Optical Sensing", IEEE MTT-S Texas 2019.

[23] S. Wane, et al., "Unification of instrumentation and EDA tooling platforms for enabling smart chip-package-PCB-probe arrays co-design solutions using advanced RFIC technologies," in IEEE Conf. on Antenna Measurements Applications, Sept. 2018, pp. 1–4.

[24] M. Bodehou, , C. Craeye, and I. Huynen, "Multifrequency band synthesis of modulated metasurface antennas", IEEE Antennas Wireless Propag. Lett. 19, 134–138 (2020).

[25] M. Bodehou, E. Martini, S. Maci, I. Huynen and C. Craeye, "Multibeam and beam scanning with modulated metasurfaces," *IEEE Trans. Antennas Propag*. vol. 68, no. 3, pp. 1273-1281, Mar. 2020.

[26] Bich-Yen Nguyen, et al., "A Path to Energy Efficiency and Reliability for ICs: Fully Depleted Silicon-on-Insulator (FD-SOI) Devices Offer Many Advantages", IEEE Solid-State Circuits Magazine , Vol. 10 , Issue: 4 , Fall 2018.

[27] J. -M. Baracco, et al., "Ka-Band Reconfigurable Reflectarrays Using Varactor Technology for Space Applications: A proposed design," in IEEE Ant. and Propag. Mag., vol. 64, no. 1, pp. 27-38, Feb. 2022.

[28] https://fr.mathworks.com/products.html.